






Giant piezoelectricity in group-IV monochalcogenides with ferroelectric AA layer stacking

Seungjun Lee ¹, Hyeong-Ryul Kim ², Wei Jiang ¹, Young-Kyun Kwon ^{2,3,*} and Tony Low ^{1,†}
¹Department of Electrical and Computer Engineering, *University of Minnesota*, Minneapolis, Minnesota 55455, USA
²Department of Physics and Research Institute for Basic Sciences, *Kyung Hee University*, Seoul 02447, Korea
³Department of Information Display, *Kyung Hee University*, Seoul 02447, Korea



(Received 16 February 2024; revised 1 May 2024; accepted 3 May 2024; published 23 May 2024)

The piezoelectricity of group-IV monochalcogenides (MX_s , with $M = \text{Ge, Sn}$ and $X = \text{S, Se}$) has attracted much attention due to their substantially higher piezoelectric coefficients compared to other 2D materials. However, with increasing layer number, their piezoelectricity rapidly disappears due to the antiferroelectric stacking order, severely limiting their practical applications. Using first-principles calculations, we investigated the piezoelectricity of MX_s with the ferroelectric AA stacking configuration, which has recently been stabilized in experiments. We found that AA-stacked MX_s have a ferroelectric ground state with the smallest lattice constant among other stacking configurations, resulting in a giant piezoelectric coefficient, which is the first demonstration of a strategy where the piezoelectric coefficients can increase with the number of layers. This can be attributed to a strong negative correlation between the lattice constant along the armchair direction and the piezoelectric coefficient, and spontaneous compressive strain stabilized in ferroelectric AA stacking configuration.

DOI: [10.1103/PhysRevB.109.195429](https://doi.org/10.1103/PhysRevB.109.195429)

I. INTRODUCTION

An interesting connection between mechanical energy and electricity in piezoelectric materials makes them highly valuable in various applications, such as energy harvesting, sensors, and optoelectronic devices [1–3]. Moreover, two-dimensional piezoelectric materials (2DPMs) are of practical interest compared to their bulk counterparts due to their flexible crystal structures and the possibility of reducing device size [4–6]. Therefore, many efforts contributed in the last decade have led to the discovery of various types of monolayer or one-layer (1L) piezoelectric materials such as hexagonal (h-) group III-IV materials [7], h-group II oxides [8], H-phase transition metal dichalcogenides (TMDs) [9,10], In_2Se_3 [11,12], CuInP_2S_6 [13,14], NbOX_2 ($X = \text{Cl, Br, and I}$) [15,16], and group IV monochalcogenides (MX_s , with $M = \text{Ge, Sn}$ and $X = \text{S, Se}$) [17–21]. Among the various candidates, MX_s , in particular, have received much attention due to their piezoelectric coefficients, which surpass those of other two-dimensional materials by orders of magnitude.

Despite these promising advancements, the practical utilization of 2DPMs has been limited because, although a few 2DPMs exhibit ferroelectric stacking order [15,16], in most 2DPMs, ground-state multilayer stacking configurations often lose their piezoelectric response [9,22]. The challenge arises from the interlayer dipole-dipole interactions, which naturally favor an antiparallel order, resulting in the restoration of spatial inversion symmetry. Nevertheless, recent advances in

materials handling and various growth techniques have paved the way for the experimental stabilization of metastable stacking configurations [20,23], resulting in novel ferroelectric (FE) order in 2DPMs. For example, interlayer twisting [24,25] or sliding [21,26,27] give rise to additional out-of-plane FE order, which is not possible in a 1L or minimum energy stacking configuration. However, despite the fact that in-plane ferroelectricity is also crucial for piezoelectric response, there is limited understanding of the effect of interlayer interactions on the in-plane FE order and the corresponding piezoelectric response.

Through first-principles calculation based on density functional theory (DFT), we investigated the stacking-dependent piezoelectric responses of MX_s . We first carefully evaluated the piezoelectric coefficients of monolayer MX to understand the large variations in their piezoelectric coefficients reported previously. We found that an in-plane lattice constant (LC) along the armchair direction primarily controls the piezoelectric coefficients of MX due to the unique puckered structures. We further revealed that, the choice of van der Waals (vdW) correction is particularly crucial for MX_s , as it significantly affects their in-plane lattice constants not only in multilayer cases but also in the 1L limit, which is not expected for other 2D materials. Therefore, we investigated the piezoelectric coefficients of AA and AC stacked MX with carefully chosen vdW corrections. We found a significant enhancement of the piezoelectric coefficients in AA stacked MX regardless of the choice of vdW corrections. The physical origin of this enhancement is a spontaneous compressive strain emerging in the AA stacking. Our results provide a deeper understanding of the piezoelectric responses of MX_s and pave the way for a novel approach to optimize the piezoelectricity in 2DPMs through stacking configuration.

*ykkwon@khu.ac.kr

†tlow@umn.edu

II. COMPUTATIONAL DETAILS

The first-principles DFT calculation [28] was carried out using Vienna *ab initio* simulation package (VASP) [29]. We employed the plane wave basis to expand the electronic wave functions with a kinetic energy cutoff of 500 eV. The projector-augmented wave pseudopotentials [30,31] were used for the valence electrons, and the exchange-correlation (XC) functional was treated within the generalized gradient approximation of Perdew-Burke-Ernzerhof (PBE) [32]. A sufficiently large vacuum region (>20 Å) was included in the unit cell to avoid any spurious interlayer interactions. The atomic basis was carefully relaxed until the Hellmann-Feynman force acting on every atom was smaller than 0.001 eV/Å, which is very crucial to get a converged piezoelectric coefficient. The Monkhorst-Pack $21 \times 21 \times 1$ k mesh was used to sample the Brillouin zone. To comprehensively investigate the effects of interlayer interactions, we used various types of vdW interactions including, simple Grimme methods [33,34], as well as various nonlocal vdW-DF functionals [35–38].

The spontaneous polarization, P , of various MX s were calculated in the framework of the modern theory of polarization based on the Berry phase [39]. Then, the planar elastic stiffness coefficients C_{ij} and piezoelectric stress coefficients e_{ijk} were evaluated as [17]

$$C_{33} = \frac{1}{A_0} \frac{\partial^2 U}{\partial \varepsilon_{33}^2}, \quad C_{22} = \frac{1}{A_0} \frac{\partial^2 U}{\partial \varepsilon_{22}^2}, \quad C_{32} = \frac{1}{A_0} \frac{\partial^2 U}{\partial \varepsilon_{33} \partial \varepsilon_{22}}, \quad (1)$$

$$e_{ijk} = \left(\frac{\partial P_i}{\partial \varepsilon_{jk}} \right)_E = \left(\frac{\partial \varepsilon_{jk}}{\partial E_i} \right)_\sigma, \quad (2)$$

where ε , σ , E , U , and A_0 are the strain, the stress, the external electric field, the total energy, and the unitcell area. The effective thickness of the 1L MX s was treated as half of the out-of-plane LC of their bulk counterparts, which was used to evaluate an effective bulk polarization. Then, the piezoelectric strain coefficients d_{ij} can be calculated as [17]

$$d_{333} = \frac{e_{333}C_{22} - e_{322}C_{32}}{C_{33}C_{22} - C_{32}^2} = \left(\frac{\partial P_3}{\partial \sigma_{33}} \right)_E = \left(\frac{\partial \varepsilon_{33}}{\partial E_3} \right)_\sigma, \quad (3)$$

$$d_{332} = \frac{e_{322}C_{33} - e_{333}C_{32}}{C_{33}C_{22} - C_{32}^2} = \left(\frac{\partial P_3}{\partial \sigma_{22}} \right)_E = \left(\frac{\partial \varepsilon_{22}}{\partial E_3} \right)_\sigma. \quad (4)$$

Using the Voigt notation, we simplify the notation as $e_{33} = e_{333}$, $e_{32} = e_{322}$, $d_{33} = d_{333}$, and $d_{32} = d_{322}$.

III. RESULTS AND DISCUSSION

Figure 1(a) shows the crystal structure of a typical 1L MX . We set z and y axes as in-plane directions with corresponding LCs of c and b , and x axis as out-of-plane direction. This choice aligns a polar direction along “ z ” or “3” direction, which follows the crystallographic conventions for orthorhombic symmetry [40]. It has puckered atomic structures with a mirror plane of M_y and belongs to $Pmn2_1$ space group [18]. More importantly, its broken M_x symmetry leads to a nonzero spontaneous polarization P along the x or armchair direction. Indeed, the spontaneous polarization of 1L MX s can be understood as a rearrangement of the atomic basis

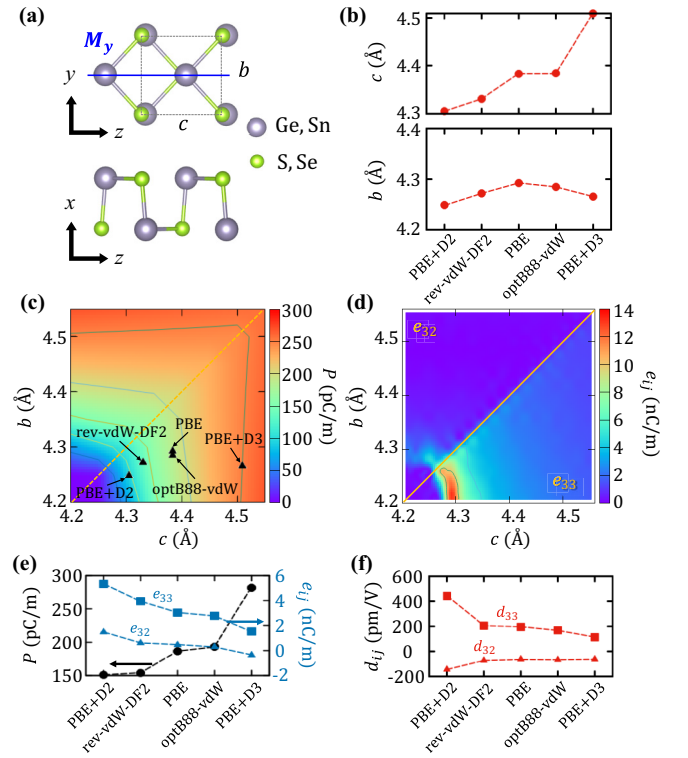


FIG. 1. (a) Top and side views of a typical monolayer (1L) group IV monochalcogenides (MX s with $M = \text{Ge}$ or Sn and $X = \text{S}$ or Se) crystal structure. (b) Lattice constants, c and b , of 1L SnSe obtained from different van der Waals (vdW). (c) Spontaneous polarization P contour map of 1L SnSe, calculated by the PBE functional without vdW correction. Equilibrium lattice constants shown in (b) were overlaid for comparison. (d) 2D piezoelectric stress coefficient (e_{ij}) contour map of 1L SnSe calculated by the derivative of (c) with strain along c . As a result, the upper left and lower right triangles represent e_{33} and e_{32} , respectively. (e) P and e_{ij} , and (f) piezoelectric strain coefficients (d_{ij}) of 1L SnSe obtained from different vdW functionals.

along the armchair direction. It has also been reported that the LC along the armchair direction plays a significant role in determining its P [19]. Therefore, we begin with our discussion on the LCs of 1L MX s using SnSe as an exemplary material and will carefully re-examine its piezoelectric coefficients.

Although the LCs of bulk MX s have been experimentally reported [41–43], those of 1L MX s have not yet been done but are only available through DFT calculations. In most previous studies [17,19,21], the LCs of 1L MX s have been obtained only with the PBE XC functional without vdW corrections, which were considered only in the multilayer case. This is the most common approach to determine the LCs of various 2D materials, since the effect of the vdW correction may be negligible in the 1L case, see the Supplemental Material [44]. However, we found that the LC of 1L SnSe strongly depends on the choice of vdW correction, as shown in Fig. 1(b). For example, the LC, c , obtained along the armchair direction ranges from 4.509 Å (PBE+D3) to 4.305 Å (PBE+D2), representing a deviation of almost 5%. Such deviation is attributed to its puckered structure with a weak stiffness along the armchair direction.

TABLE I. Lattice constants, a and b , spontaneous polarization, P , piezoelectric stress coefficients, e_{ij} , planar elastic stiffness coefficients, C_{ij} , and piezoelectric strain coefficients, d_{ij} of 1L SnSe calculated by various functionals.

vdW	$c(\text{\AA})$	$b(\text{\AA})$	$P(\text{pC/m})$	$e_{33}(\text{nC/m})$	$e_{32}(\text{nC/m})$	$C_{33}(\text{N/m})$	$C_{22}(\text{N/m})$	$C_{32}(\text{N/m})$	$d_{33}(\text{pm/V})$	$d_{32}(\text{pm/V})$
none (PBE)	4.383	4.292	186.3	3.01	0.46	21.47	44.73	17.6	194.50	-66.25
none (PBE) [17]	4.35	4.24		3.49	1.08	19.88	44.49	18.57	250.57	-80.31
none (PBE) [18]	4.36	4.30		2.47	-0.05					
none (PBE) [45]	4.41	4.29		2.81	0.52	23.06	42.82	18.89	175.32	-65.11
none (PBE) [19]			181							
D3	4.509	4.265	281.7	1.50	-0.36	25.47	42.06	21.02	112.29	-64.61
D2	4.305	4.248	150.6	5.31	1.46	17.85	41.64	17.24	439.27	-146.81
optB88	4.384	4.284	192.5	2.74	0.27	25.02	45.00	20.26	164.7	-68.15
optB88 [46]	4.41	4.27		2.35	0.76	20	40.4	17	158.2	-47.7
rev-vdW-DF2	4.331	4.271	153.8	3.91	0.59	26.61	47.6	20.19	202.8	-73.62
vdW-TS [18]	4.37	4.27		3.08	0.21					

We found that a small change in the LCs of 1L MX s would cause a large variation in their piezoelectric coefficients. To understand this result, we calculated P of 1L SnSe as a function of the two in-plane lattice constants c and b using PBE XC, which is shown as a contour map in Fig. 1(c), where other calculated LCs using other functions are superimposed. The contour map is symmetric with respect to the $c = b$ line with C_4 rotational symmetry due to the degenerate ground states for $c > b$ and $c < b$. As clearly visualized in Fig. 1(c), P is positively correlated with c , and the aspect ratio between c and b also has some secondary effects. As the LC decreases, 1L SnSe loses its P and becomes paraelectric. Therefore, the vdW correction, which yields a smaller (larger) LC along the armchair direction, may underestimate (overestimate) P . For example, the P value of 281.7 pC/m estimated with the PBE+D3 correction is almost twice the value of 150.6 pC/m estimated with the PBE+D2 correction. Figure 1(d) shows the contour map of the 2D piezoelectric stress coefficients, e_{ij} , computed by taking the first derivative of P shown in Fig. 1(c) with respect to strain ε_{jk} , as explained in the computational details and Supplemental Material [44]. We found significantly stronger e_{33} near the boundary between the paraelectric and FE phases due to the rapid emergence of nonzero P , and a small enhancement in e_{32} , although much smaller than e_{33} . This result clearly indicates that a compressive strain along the armchair direction may play a major role in the enhancement of e_{33} of SnSe. Simultaneously, it also implies that the fluctuation of the LC according to the choice of vdW functionals makes a large uncertainty in predicting its piezoelectric coefficients. Note that, while e_{33} is always positive in MX s, e_{32} can be either positive or negative. Physically, negative e_{32} indicates that P decreases when aspect ratio “ c/b ” between two lattice constants becomes larger.

For a more systematic study, we evaluated the piezoelectric coefficients of 1L SnSe using various vdW functionals, as summarized in Figs. 1(e) and 1(f), and Table I. Due to the strong correlation between P and a , both the stress and strain piezoelectric coefficients (e_{ij} and d_{ij}) also strongly depend on the choice of functional. For example, e_{33} and d_{33} range from 5.31 nC/m to 1.50 nC/m, and from 439.27 pm/V to 112.29 pm/V, respectively. As predicted above, the smaller c leads to the higher e_{ij} and d_{ij} . We further confirmed that our results are consistent with previously reported studies,

and the observed variation in both e_{ij} and d_{ij} is simply understood as the result of variation in the relaxed c . We also confirmed that the differences in the piezoelectric coefficients evaluated with different vdW functionals are due predominantly to the different equilibrium LCs predicted by the different vdW functionals, with other factors such as differences in atomic relaxations having a smaller effect [44]. Therefore, we emphasize that the choice of computational options is extremely important in the quantitative analysis and the vdW functional should be used consistently in both 1L and multilayer cases.

A careful investigation in the previous section indicates that there is a significant uncertainty in determining the exact value of the piezoelectric coefficients of 1L MX s without experimental input of LCs. Therefore, before investigating the piezoelectric coefficients of multilayer MX s, we calculated the LCs of bulk MX s, and then compared them with experimentally available values to validate which vdW correction is most appropriate among various vdW functionals. Figure 2 shows the LCs of four different bulk MX s calculated with seven different functionals (red dots) together with their experimental values (red solid lines) for comparison. Among various functionals, the rev-vdW-DF2 method shows better agreement with experimental values than the other functionals [44]. Therefore, here, we primarily use the rev-vdW-DF2 vdW correction in investigating piezoelectric coefficients of 1L and multilayer MX s. For a better understanding, we also repeated all calculations using the Grimme-D3 vdW corrections [44]. Note that, all physical results are qualitatively consistent when using the same vdW functionals for both 1L and multilayer cases, regardless of which vdW functionals were used. However, the conventional approach (i.e., vdW functional is only considered in multilayers) may lead to misinterpretation of the results, which will be discussed later.

Figures 3(a) and 3(b) show antiferroelectric (AFE) and FE stacking orders and four possible sliding configurations. Thus, there are a total of eight possible stacking configurations. Although it is known that the ground state stacking configuration of MX s is the AFE AB stacking [20,21], it has also been predicted that the FE order can be stabilized in both the AA and AC stacking configurations [21]. In addition, it has been experimentally confirmed that the AA-stacked FE SnS can exist on a mica substrate below a certain critical thickness

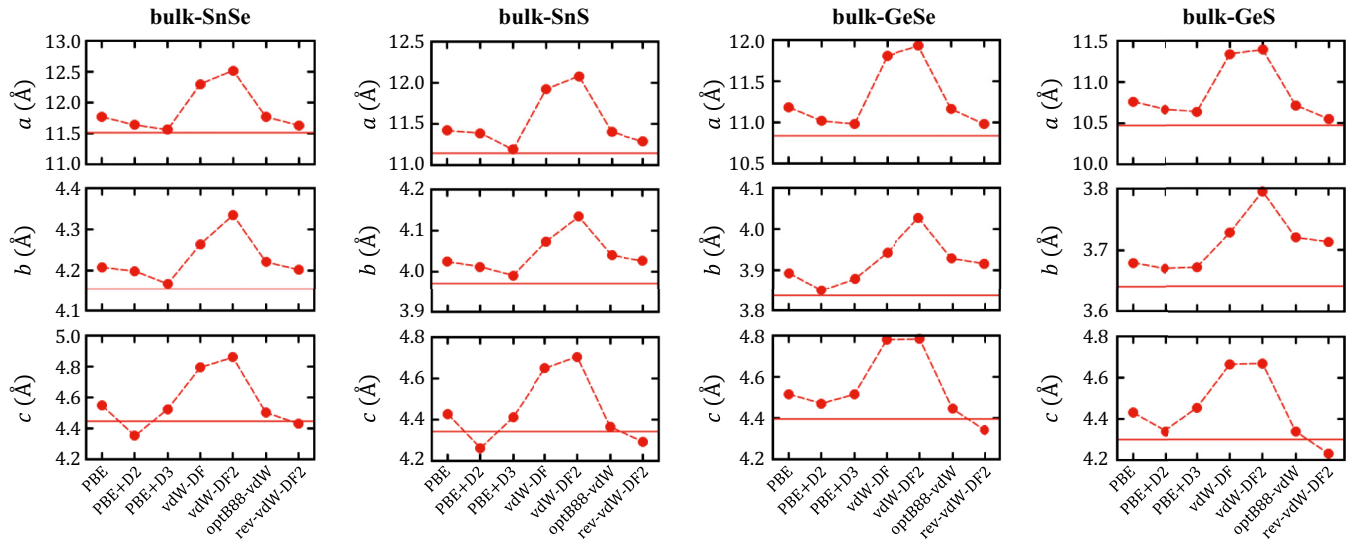


FIG. 2. Calculated lattice constants of bulk group IV monochalcogenides, obtained using various van der Waals corrections (red dots). Experimental values obtained from Ref. [41–43] are also shown as red solid lines for comparison.

[20]. Therefore, here, we first focus on 2L AA and AC stacked SnSe to understand the FE order in multilayer *MX*s.

Figures 3(c) and 3(d) show the P contour maps of FE 2L SnSe in AA and AC stacking configurations, respectively. Overall shapes of both contour maps are very similar with those of their 1L counterparts shown in Fig. 1(c) with twice larger P values. Although AC stacking exhibits a slightly stronger P compared to AA stacking, the relative difference is not significant. This means that the P of 2L SnSe is mainly due

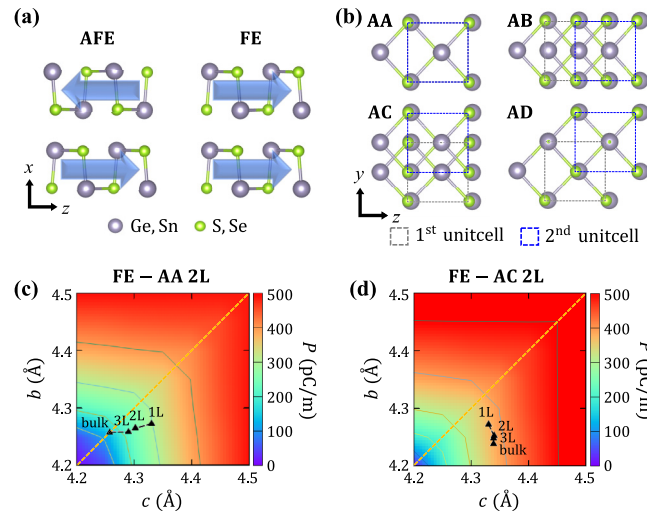


FIG. 3. (a) Side views of antiferroelectric (AFE) and ferroelectric (FE) stacking configurations of bilayer *MX* and (b) top views of four possible in-plane sliding configurations. In (a), blue arrows indicate the direction of the spontaneous polarization of each layer. In (b) grey and blue dashed rectangles visualize unit cells of each layer. (c) Contour maps of the spontaneous polarization P of the FE 2L SnSe in (c) AA and (d) AC stacking configurations calculated by PBE with the rev-vdW-DF2 vdW correction. Equilibrium lattice constants of 1L, 2L, 3L, and bulk AA and AC SnSe are overlaid on (c) and (d), respectively.

to the intralayer contribution in both configurations. Therefore, similar to the 1L case, the equilibrium LCs primarily determine their P . The obtained LCs of multilayer SnSe were overlaid in Figs. 3(c) and 3(d). The LCs of 2L AA SnSe were evaluated to be $c = 4.302$ Å and $b = 4.263$ Å, whereas those of 2L AC phase are $c = 4.340$ Å and $b = 4.251$ Å. Especially we focus on change in c along the armchair direction when stacked from 1L to 2L. As shown in Figs. 3(c) and 3(d), where the LCs of SnSe with different number of layers are overlaid, AA stacking significantly reduces c , while AC stacking does not change c considerably, compared to the 1L case. Thus, 2L AA SnSe has a smaller P and may have a larger e_{ij} than 2L AC SnSe. It is worth noting that the reduction of LCs of 2L AA SnSe can be understood as a result of dipole-dipole interactions. Since parallel dipole-dipole interaction is inherently unfavorable, relaxed structures can form in ways that favor either a decrease in P or an increase in the P - P distance. Notably, this result remains robust across different vdW functionals and is thus applicable to other *MX*s, emphasizing the generalizability of the observed phenomenon [44].

Figure 4 shows the variation of four available piezoelectric coefficients (e_{33} , e_{32} , d_{33} , and d_{32}) of SnSe with the number of layers up to 3L in AA, AB, and AC stacking configurations [44]. For the AB stacking configuration, due to its AFE order, the piezoelectric coefficients of the even-numbered layers are calculated to be zero, and those of the odd-numbered layers are also smaller than those of the monolayer. On the other hand, the 2D piezoelectric stress coefficients (e_{33} and e_{32} , in the unit of nC/m) increase with the number of layers in both AA and AC stacking configurations. Moreover, AA stacking exhibits higher piezoelectric coefficients than AC stacking, which is consistent with our prediction based on the LCs. For example, the e_{33} of 3L AA SnSe was calculated to be 13.5 nC/m which is larger than that of AC SnSe (8.53 nC/m), and also six times larger than that of 3L AB SnSe (2.39 nC/m). By definition of 2D piezoelectric stress coefficients, n times enhancement in nL indicates that the intralayer contribution is the same as in the monolayer case. As shown in Fig. 4(a), the

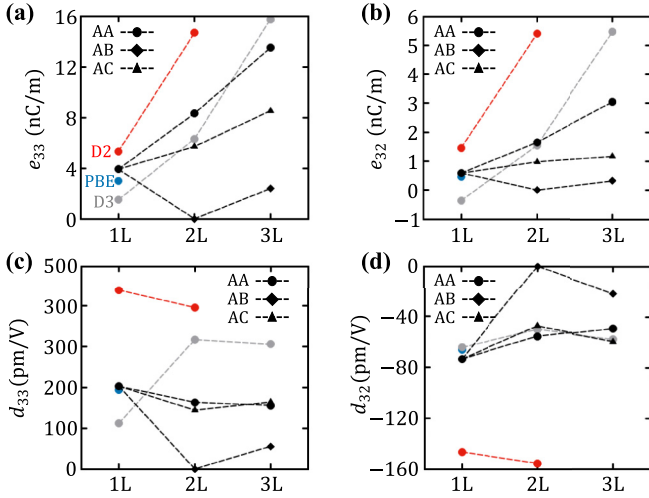


FIG. 4. 2D piezoelectric stress coefficients (a) e_{33} and (b) e_{32} , and piezoelectric strain coefficients (c) d_{33} and (d) d_{32} of 1L, 2L, and 3L SnSe with AA, AB, and AC stacking configurations, calculated with the rev-vdW-DF2 vdW correction (black). For comparison, the results of the Grimme-D3 (grey), Grimme-D2 (red), and PBE (blue) are also shown for the AA SnSe and 1L SnSe, respectively.

e_{33} of 2L and 3L AA SnSe were calculated to be 8.32 nC/m and 13.50 nC/m, which are 213% and 345% of that of 1L, indicating additional enhancement from the intralayer contribution due to the spontaneous compressive strain. In other words, the effective bulk piezoelectric coefficient (C/m^2) of 3L AA SnSe is also 15% larger than that of 1L SnSe thanks to the smaller LC.

However, the other important coefficients, the piezoelectric strain coefficients (d_{33} and d_{32}) of multilayer AA SnSe are more sensitive to the choice of vdW correction, and do not exhibit consistent trends with the number of layers. For example, while the d_{33} of 2L AA SnSe decreases slightly compared to 1L SnSe when evaluated with the rev-vdW-DF2 vdW correction, it is predicted to increase threefold when evaluated with the Grimme-D3 correction. Therefore, it is difficult to say that both d_{33} and d_{32} generally increase in the AA stacking configuration. It is worth noting that although there is no meaningful improvement in d_{33} and d_{32} in multilayer AA MXs compared to 1L, these values are much larger than those of AB MXs. For example, the d_{33} of 3L AA SnSe (155.96 pm/V) is almost three times larger than that of 3L AB SnSe (55.2 pm/V), suggesting that AA stacking MX is a promising candidate in piezoelectric applications. For all other AA MXs, we also calculated e_{33} , e_{32} , d_{33} , and d_{32} up to 2L using both rev-vdW-DF2 and Grimme-D3 corrections [44]. We consistently found that as the LC decreases, e_{33} and e_{32} continue to enhance, while d_{33} and d_{32} remain comparable to those of 1L MXs.

As shown in Fig. 3(c), the LC c of AA SnSe continues to shrink with stacking, but the bulk AA SnSe loses P and becomes paraelectric, implying that there exists a critical thickness below which nonzero P is accommodated. In fact, a previous experiment has successfully grown AA SnS on mica substrates, exhibiting room temperature ferroelectricity up to 15 layers [20], indicating that the critical thickness is not too

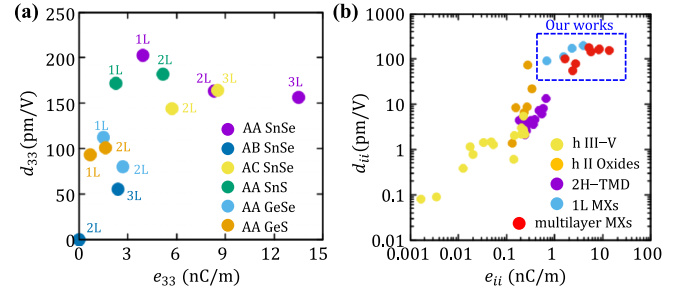


FIG. 5. Summarized piezoelectric coefficients of (a) group IV monochalcogenides (MXs) and (b) various 2D materials calculated by rev-vdW-DF2 functional. In (a) purple, dark-blue, yellow, green, skyblue, and orange circles represent AA (stacking) SnSe, AB SnSe, AC SnSe, AA SnS, AA GeSe, and AA GeS, respectively. In (b) yellow, orange, and purple circles denote materials of hexagonal Group III-V (h III-V), hexagonal Group II oxides (h II Oxides), and H phase transition metal dichalcogenides (2H-TMD), respectively, obtained from Ref. [8]. Skyblue and red circles surrounded by a blue dashed rectangle denote our results of 1L MXs and multilayer MXs.

thin and could be further optimized by adjusting the experimental conditions. This observation supports our prediction of optimizing the piezoelectric coefficients of multilayer MXs by utilizing AA stacking configuration.

Finally, we summarize the piezoelectric coefficients of multilayer MXs, as shown in Fig. 5(a). SnSe shows the highest e_{33} and d_{33} , followed by SnS, GeSe, and GeS. In all MXs, the AA stacking boasts higher e_{33} than any other stacking, while d_{33} is more or less than that of the corresponding 1L case regardless of the stacking configuration. In addition to e_{33} and d_{33} , other physical properties such as stability and switching barrier between the FE and AFE phases are also important in piezoelectric applications. Therefore, all MXs can be practically useful, and utilizing AA stacking configuration is an efficient way to optimize their piezoelectric response.

For comparison, we also summarized the piezoelectric coefficients of several other 2D materials, as shown in Fig. 5(b). Consistent with the previous reports, we observed that 1L MXs have exceptionally large piezoelectric coefficients compared to the other 2D materials, even larger coefficients in AA stacked MXs. It is worthy of note that the giant piezoelectric coefficients observed in AA MXs not only stand out among 2D materials, but are also comparable to bulk piezoelectric materials. Recent high-throughput DFT calculations revealed that among 941 bulk piezoelectric materials, only 5% of materials satisfy $|e_{ij}| > 3 C/m^2$, including experimentally confirmed giant piezoelectric materials such as BaTiO₃ (3.49 C/m²), SrHfO₃ (8.73 C/m²), RbTaO₃ (8.93 C/m²), and BaNiO₃ (27.46 C/m²) [48]. Using the effective thickness of 1.74 nm (1.74 nm = 1.5 c , c is an out-of-plane lattice constant of bulk SnSe), the effective bulk e_{33} value of 3L AA SnSe was calculated to be 7.76 C/m², which is even larger than that of BaTiO₃. Within the Grimme-D2 vdW correction, the e_{33} of 2L AA SnSe was estimated to be 12.66 C/m² (14.68 nC/m). It is even larger than not only that of 3L AA SnSe estimated by rev-vdW-DF2, but also that of SrHfO₃ and RbTaO₃. We now conclude that our theoretical calculations

have undoubtedly revealed that there is a strong correlation between the reduction of LCs and giant piezoelectric coefficients in AA-stacked MXs, regardless of the vdW functional used, making it a promising candidate for low-dimensional piezoelectric applications.

IV. CONCLUSION

In summary, we have used first-principles calculations to study the piezoelectric coefficients of multilayer MXs with AA and AC stacking configurations, which are known to stabilize ferroelectric order. Our re-examination of 1L MXs revealed the pivotal role of the van der Waals interaction in ensuring accurate and reliable predictions of piezoelectric coefficients. Through systematic DFT calculations, we found that the AA-stacked configurations exhibit remarkably larger piezoelectric coefficients compared to all reported layered materials, including their monolayer counterparts. The origin of this enhancement lies in the compressive strain along the

armchair direction, which is spontaneously introduced in the ferroelectric AA stacking. These findings not only provide a comprehensive understanding of the piezoelectric behavior of MXs, but also suggest a novel strategy for optimizing piezoelectricity in low-dimensional materials through stacking configuration.

ACKNOWLEDGMENTS

S.L., W.J., and T.L. were supported by the National Science Foundation (NSF) through the DMREF program under Award No. DMR-1921629. S.L. is also supported by Basic Science Research Program through the National Research Foundation of Korea (NRF) funded by the Ministry of Education (NRF-2021R1A6A3A14038837). H.-R.K. and Y.-K.K. acknowledge financial support from the Korean government through the NRF (NRF-2022R1A2C1005505, NRF-2022M3F3A2A01073562). The computational work was partially done using the resources of the KISTI Supercomputing Center (KSC-2023-CRE-0053).

-
- [1] Z. L. Wang and J. Song, Piezoelectric nanogenerators based on zinc oxide nanowire arrays, *Science* **312**, 242 (2006).
- [2] Z. L. Wang, Nanopiezotronics, *Adv. Mater.* **19**, 889 (2007).
- [3] R. Bao, J. Tao, C. Pan, and Z. L. Wang, Piezophotronic effect in nanosensors, *Small Sci.* **1**, 2000060 (2021).
- [4] R. Hinchet, U. Khan, C. Falconi, and S.-W. Kim, Piezoelectric properties in two-dimensional materials: Simulations and experiments, *Mater. Today* **21**, 611 (2018).
- [5] Q. Zhang, S. Zuo, P. Chen, and C. Pan, Piezotronics in two-dimensional materials, *InfoMat* **3**, 987 (2021).
- [6] C.-C. Jin, D.-M. Liu, and L.-X. Zhang, An emerging family of piezocatalysts: 2D piezoelectric materials, *Small* **19**, 2303586 (2023).
- [7] P. Ares, T. Cea, M. Holwill, Y. B. Wang, R. Roldán, F. Guinea, D. V. Andreeva, L. Fumagalli, K. S. Novoselov, and C. R. Woods, Piezoelectricity in monolayer hexagonal boron nitride, *Adv. Mater.* **32**, 1905504 (2020).
- [8] M. N. Blonsky, H. L. Zhuang, A. K. Singh, and R. G. Hennig, Ab initio prediction of piezoelectricity in two-dimensional materials, *ACS Nano* **9**, 9885 (2015).
- [9] H. Zhu, Y. Wang, J. Xiao, M. Liu, S. Xiong, Z. J. Wong, Z. Ye, Y. Ye, X. Yin, and X. Zhang, Observation of piezoelectricity in free-standing monolayer MoS₂, *Nat. Nanotechnol.* **10**, 151 (2015).
- [10] M. M. Alyoruk, Y. Aierken, D. Çakır, F. M. Peeters, and C. Sevik, Promising piezoelectric performance of single layer transition-metal dichalcogenides and dioxides, *J. Phys. Chem. C* **119**, 23231 (2015).
- [11] Y. Zhou, D. Wu, Y. Zhu, Y. Cho, Q. He, X. Yang, K. Herrera, Z. Chu, Y. Han, M. C. Downer *et al.*, Out-of-plane piezoelectricity and ferroelectricity in layered α -In₂Se₃ nanoflakes, *Nano Lett.* **17**, 5508 (2017).
- [12] F. Xue, J. Zhang, W. Hu, W.-T. Hsu, A. Han, S.-F. Leung, J.-K. Huang, Y. Wan, S. Liu, J. Zhang *et al.*, Multidirection piezoelectricity in mono- and multilayered hexagonal α -In₂Se₃, *ACS Nano* **12**, 4976 (2018).
- [13] F. Liu, L. You, K. L. Seyler, X. Li, P. Yu, J. Lin, X. Wang, J. Zhou, H. Wang, H. He *et al.*, Room-temperature ferroelectricity in CuInP₂S₆ ultrathin flakes, *Nat. Commun.* **7**, 12357 (2016).
- [14] J. A. Brehm, S. M. Neumayer, L. Tao, A. O'Hara, M. Chyasnovich, M. A. Susner, M. A. McGuire, S. V. Kalinin, S. Jesse, P. Ganesh *et al.*, Tunable quadruple-well ferroelectric van der Waals crystals, *Nat. Mater.* **19**, 43 (2020).
- [15] Y. Jia, M. Zhao, G. Gou, X. C. Zeng, and J. Li, Niobium oxide dihalides NbOX₂: A new family of two-dimensional van der Waals layered materials with intrinsic ferroelectricity and antiferroelectricity, *Nanoscale Horizons* **4**, 1113 (2019).
- [16] Y. Wu, I. Abdelwahab, K. C. Kwon, I. Verzhbitskiy, L. Wang, W. H. Liew, K. Yao, G. Eda, K. P. Loh, L. Shen *et al.*, Data-driven discovery of high performance layered van der Waals piezoelectric NbOI₂, *Nat. Commun.* **13**, 1884 (2022).
- [17] R. Fei, W. Li, J. Li, and L. Yang, Giant piezoelectricity of monolayer group IV monochalcogenides: SnSe, SnS, GeSe, and GeS, *Appl. Phys. Lett.* **107**, 173104 (2015).
- [18] L. C. Gomes, A. Carvalho, and A. H. Castro Neto, Enhanced piezoelectricity and modified dielectric screening of two-dimensional group-IV monochalcogenides, *Phys. Rev. B* **92**, 214103 (2015).
- [19] H. Wang and X. Qian, Two-dimensional multiferroics in monolayer group IV monochalcogenides, *2D Mater.* **4**, 015042 (2017).
- [20] N. Higashitarumizu, H. Kawamoto, C.-J. Lee, B.-H. Lin, F.-H. Chu, I. Yonemori, T. Nishimura, K. Wakabayashi, W.-H. Chang, and K. Nagashio, Purely in-plane ferroelectricity in monolayer SnS at room temperature, *Nat. Commun.* **11**, 2428 (2020).
- [21] B. Xu, J. Deng, X. Ding, J. Sun, and J. Z. Liu, Van der Waals force-induced intralayer ferroelectric-to-antiferroelectric transition via interlayer sliding in bilayer group-IV monochalcogenides, *Npj Comput. Mater.* **8**, 47 (2022).
- [22] Y. Li, Y. Rao, K. F. Mak, Y. You, S. Wang, C. R. Dean, and T. F. Heinz, Probing symmetry properties of few-layer MoS₂ and h-BN by optical second-harmonic generation, *Nano Lett.* **13**, 3329 (2013).

- [23] H. Yoo, R. Engelke, S. Carr, S. Fang, K. Zhang, P. Cazeaux, S. H. Sung, R. Hovden, A. W. Tsun, T. Taniguchi *et al.*, Atomic and electronic reconstruction at the van der Waals interface in twisted bilayer graphene, *Nat. Mater.* **18**, 448 (2019).
- [24] C. Woods, P. Ares, H. Nevison-Andrews, M. Holwill, R. Fabregas, F. Guinea, A. Geim, K. Novoselov, N. Walet, and L. Fumagalli, Charge-polarized interfacial superlattices in marginally twisted hexagonal boron nitride, *Nat. Commun.* **12**, 347 (2021).
- [25] K. Yasuda, X. Wang, K. Watanabe, T. Taniguchi, and P. Jarillo-Herrero, Stacking-engineered ferroelectricity in bilayer boron nitride, *Science* **372**, 1458 (2021).
- [26] P. Meng, Y. Wu, R. Bian, E. Pan, B. Dong, X. Zhao, J. Chen, L. Wu, Y. Sun, Q. Fu *et al.*, Sliding induced multiple polarization states in two-dimensional ferroelectrics, *Nat. Commun.* **13**, 7696 (2022).
- [27] S. Deb, W. Cao, N. Raab, K. Watanabe, T. Taniguchi, M. Goldstein, L. Kronik, M. Urbakh, O. Hod, and M. Ben Shalom, Cumulative polarization in conductive interfacial ferroelectrics, *Nature (London)* **612**, 465 (2022).
- [28] W. Kohn and L. J. Sham, Self-consistent equations including exchange and correlation effects, *Phys. Rev.* **140**, A1133 (1965).
- [29] G. Kresse and J. Furthmüller, Efficient iterative schemes for *ab initio* total-energy calculations using a plane-wave basis set, *Phys. Rev. B* **54**, 11169 (1996).
- [30] P. E. Blöchl, Projector augmented-wave method, *Phys. Rev. B* **50**, 17953 (1994).
- [31] G. Kresse and D. Joubert, From ultrasoft pseudopotentials to the projector augmented-wave method, *Phys. Rev. B* **59**, 1758 (1999).
- [32] J. P. Perdew, K. Burke, and M. Ernzerhof, Generalized gradient approximation made simple, *Phys. Rev. Lett.* **77**, 3865 (1996).
- [33] S. Grimme, Semiempirical GGA-type density functional constructed with a long-range dispersion correction, *J. Comput. Chem.* **27**, 1787 (2006).
- [34] S. Grimme, J. Antony, S. Ehrlich, and H. Krieg, A consistent and accurate *ab initio* parametrization of density functional dispersion correction (DFT-D) for the 94 elements H-Pu, *J. Chem. Phys.* **132**, 154104 (2010).
- [35] M. Dion, H. Rydberg, E. Schröder, D. C. Langreth, and B. I. Lundqvist, van der Waals density functional for general geometries, *Phys. Rev. Lett.* **92**, 246401 (2004).
- [36] K. Lee, É. D. Murray, L. Kong, B. I. Lundqvist, and D. C. Langreth, Higher-accuracy van der Waals density functional, *Phys. Rev. B* **82**, 081101(R) (2010).
- [37] J. Klimeš, D. R. Bowler, and A. Michaelides, Chemical accuracy for the van der Waals density functional, *J. Phys.: Condens. Matter* **22**, 022201 (2010).
- [38] I. Hamada, van der Waals density functional made accurate, *Phys. Rev. B* **89**, 121103(R) (2014).
- [39] N. A. Spaldin, A beginner's guide to the modern theory of polarization, *J. Solid State Chem.* **195**, 2 (2012).
- [40] R. E. Newnham, *Properties of Materials: Anisotropy, Symmetry, Structure* (Oxford University Press, Oxford, 2005).
- [41] T. Chattopadhyay, J. Pannetier, and H. G. Von Schnering, Neutron diffraction study of the structural phase transition in SnS and SnSe, *J. Phys. Chem. Solids* **47**, 879 (1986).
- [42] T. Grandke and L. Ley, Angular-resolved uv photoemission and the band structure of GeS, *Phys. Rev. B* **16**, 832 (1977).
- [43] P. A. E. Murgatroyd, M. J. Smiles, C. N. Savory, T. P. Shalvey, J. E. N. Swallow, N. Fleck, C. M. Robertson, F. Jäckel, J. Alaria, J. D. Major, D. O. Scanlon, and T. D. Veal, GeSe: Optical spectroscopy and theoretical study of a van der Waals solar absorber, *Chem. Mater.* **32**, 3245 (2020).
- [44] See Supplemental Material at <http://link.aps.org/supplemental/10.1103/PhysRevB.109.195429> for details of lattice constants of other 2D materials depending on vdW functionals; computational approach in evaluating piezoelectric coefficients of group IV monochalcogenides; calculated piezoelectric coefficients of SnSe using different vdW functionals; performance of van der Waals functionals for bulk group IV monochalcogenides; tables summarizing calculated lattice constants and detailed piezoelectric coefficients of group IV monochalcogenides. Supplemental Figs. S1–S4 and Supplemental Tables S1–S6. It also contains Ref. [47].
- [45] S.-D. Guo, X.-S. Guo, Y.-Y. Zhang, and K. Luo, Small strain induced large piezoelectric coefficient in α -AsP monolayer, *J. Alloys Compd.* **822**, 153577 (2020).
- [46] W. Fang, L.-C. Zhang, G. Qin, Q.-B. Yan, Q.-R. Zheng, and G. Su, Layer dependence of geometric, electronic and piezoelectric properties of SnSe, *arXiv:1603.01791*.
- [47] G. Henkelman, B. P. Uberuaga, and H. Jónsson, A climbing image nudged elastic band method for finding saddle points and minimum energy paths, *J. Chem. Phys.* **113**, 9901 (2000).
- [48] M. de Jong, W. Chen, H. Geerlings, M. Asta, and K. A. Persson, A database to enable discovery and design of piezoelectric materials, *Sci. Data* **2**, 150053 (2015).